# Electronic structure of metal phthalocyanines on Ag (100)


## Cornelius Krull


Ph.D. Thesis

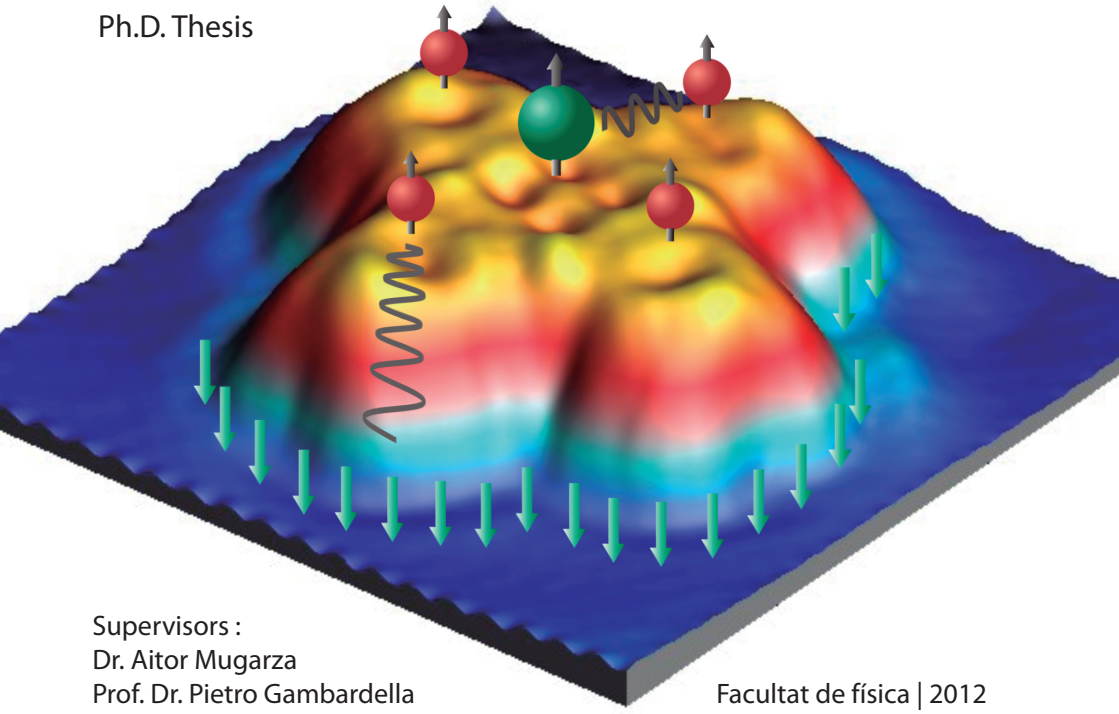


Supervisors :
Dr. Aitor Mugarza
Prof. Dr. Pietro Gambardella


Facultat de física | 2012


Institut Català de Nanotecnologia
Universitat Autònoma de Barcelona

Chapter 4

# 4 Adsorption of Metal Phthalocyanines on Ag(100)

Since its invention STM has been widely used to study molecules on surfaces. It proved an ideal tool for this purpose, giving access to both the real space adsorption geometry and electronic structure of molecular adsorbates. Copper Phthalocyanines on polycrystalline Silver were among the first molecules studied as early as 1987 [121, 122, 123]. Today many more MePc molecules on different metal surfaces have been investigated (Me = Cu [123, 121, 124, 125, 126], Co [110, 127, 126], Fe [128, 129, 111, 130, 131, 132, 133, 134], Ni [130], Pd [135], Zn [136], Mn [137, 138], Sn [139]). In general, single MePc molecules adsorb flat on the surface, and their four isoindole groups (see Figure 4.1) are imaged as a four lobed cross shape in STM topography. Depending on the character of the filled $d$ states of the metal ion, the center appears either as a dip or as a protrusion [126, 130].

The interplay between molecule-substrate interaction and molecule-molecule leads to self assembly of MePc into highly ordered clusters or layers. The substrate symmetry in relation to the four fold symmetry of the molecules can lead to to creation of domains of molecular ordering [128]. Multilayer films show a growth structure with the molecular plane parallel [140] or tilted with respect to the surface plane [128, 129]. Many growth studies on noble metal (111) surfaces have been undertaken: on Ag(111) CuPc monolayers [141], FePc up to multilayer [129], FePc sub-monolayer [142, 143], single SnPc to multilayer [139], on Au(111) MnPc and FePc sub-monolayer [137], CoPc

multilayers [144], SnPc multilayers [145], single FePc to monolayer [134] and on Cu(111) single CoPc [146, 127] and up to monolayer structures [147]. For the (100) surface studies are more scarce, to our best knowledge only CoPc [148] and NiPc/CuPc monolayers [149] on Cu(100) have been investigated .

In this chapter we present a systematical investigation of the adsorption of four different types of Metal Phthalocyanines (MePc) (Me=Fe, Co, Ni, Cu) on the Ag(100) surface. The evolution of the growth is studied step by step by STM starting from single molecules, dimers, larger clusters up to a complete monolayer, and finally multilayer structures. We find that the adsorption on the surface induces chirality in the otherwise achiral MePc molecules. Interestingly, this is not a geometric distortion, but rather an electronic effect. Our detailed study allows us to follow the evolution and transfer of chirality from the single molecule level up to the structural level, found in clusters and monolayers. The STM results are compared to DFT results, which provide further insight into electronic structure of the molecule-substrate complex. The calculations were performed by R. Robles, P. Ordejón and N. Lorente.

## 4.1. Chemical structure of Metal Phthalocyanines

MePc are coordination complexes formed by a central metal ion and an organic ligand. The chemical structure is depicted in Figure 4.1. The ligand consists of 4 isoindole groups linked by 4 aza-bridging Nitrogen atoms. The ligands are arranged around the metal ion in a cross shaped structure. The Me - Pc bond involves charge transfer from the metal to the ligand, leaving the metal in an ionized state, typically $[Me]^{2+}$ for transition metal (TM) ions.

More than 70 different metal atoms have been found to coordinate with phthalocyanines, creating a vast range of different electronic and magnetic properties. It is exactly this variety that makes them interesting for research and the application in spintronic devices. It allows for a systematic metal ion-dependent investigation of the molecular properties.

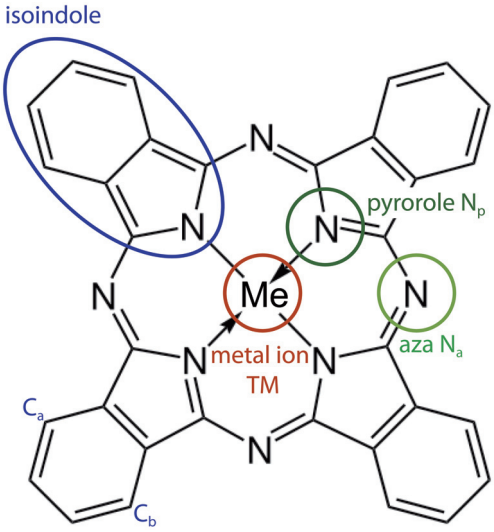


**Figure 4.1.:** The Lewis structure of a metal phthalocyanine. The ligand consists of 4 isoindole groups linked by 4 aza-bridging Nitrogen atoms. The different types of Nitrogen atoms are labeled $N_a$ and $N_p$. MePc can accommodate a large variety of metal ions. In this work the 3d metals Fe, Co, Ni and Cu are investigated. The two Carbon $C_a$ and $C_b$ atoms in the benzene rings are labeled to measure chiral distortions (See Table 4.1).

## 4.2. Adsorption of single molecules

### 4.2.1. Adsorption configuration

In this first section we will look at the adsorption geometry for single molecules of the investigated MePc (Me= Fe, Co, Ni, Cu). At first glance their behavior is very similar, although as we will see depending on the 3d level occupation of the central ion, the contributions to the molecule-surface interaction are different.

Figure 4.2 shows a topographic image of low coverage NiPc and CoPc adsorbed on Ag(100). The molecules appear as a four lobed structure, which can be easily identified as the four isoindole groups of the Pc ligand. This indicates an adsorption parallel to the surface, as seen in previous investigations [111, 123, 126, 130, 131, 146]. Based on their topographic appearance at most bias voltages, the molecules can be further classified

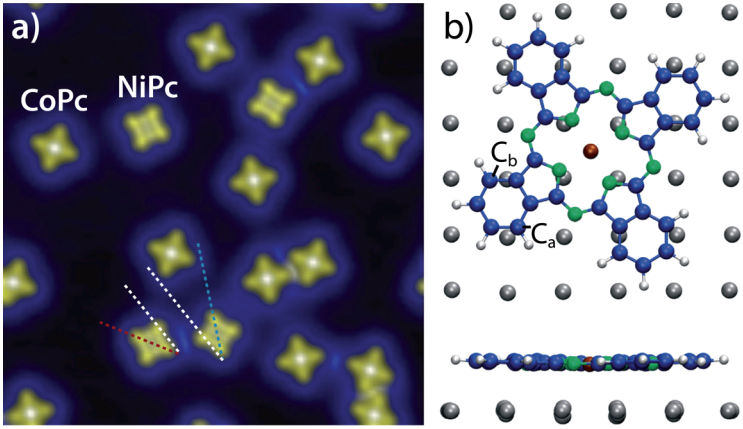


**Figure 4.2.:** a) Topographic image of CoPc and NiPc molecules codeposited at room temperature on the Ag(100) surface (13.4 nm x13.4 nm, 0.5 nA, -1.0 V) The blue/red line indicates the $\pm 30^{o}$ rotation of the molecular axis with respect to the [011] surface lattice vectors (white line) determined from atomically resolved images of the Ag surface. b) Adsorption configuration of MePc on Ag(100) as obtained from DFT. Upper panel: top view showing the hollow adsorption site. Side view: Some of the Ag atoms are shifted from their original height.

in two groups. The TM-center is either a protrusion for FePc and CoPc or a depression for NiPc and CuPc (see Figure 4.2). This difference is, however, not related to molecular structure, as confirmed by the similar adsorption configuration obtained in DFT calculations (See Table 4.1). Instead, it reflects the high or low degree of coupling between the TM's $d$ electrons near the Fermi level ($E_F$) and the substrate/tip (see chapter 5 and [130]).

Two different rotational orientations of the MePc can be identified. By comparing these to atomically resolved images of the Ag substrate, we can quantify the rotation. The ligand axis is rotated by $\pm 30^{o}$ ($\pm 2^{o}$) with respect to the [011] surface lattice vectors, similar to results found for CuPc on Cu(100) [123]. Moreover by extrapolating the surface lattice imaged next to a MePc we find that the metal ion is located over an Ag hollow site (see Figure 4.2b). The DFT calculations confirm this adsorption site with a 0.14 eV energy gain over the next stable configuration.

Additionally, DFT identifies the driving force for the azimuthal orientation of the molecular axis as the bond between the aza-Nitrogens ($N_a$) and the underlying Ag atoms. In order to minimize the $N_a$-Ag distance, the

molecule rotates its isoindole axis by 30° with respect to the [011] surface vector. Both theory and experiment find very similar, TM-indepedent, configurations for all MePcs (see Figure 4.2b), confirming the leading role of N-substrate interactions in determining the molecular orientation.

In the calculations the molecule becomes slightly concave after deposition, meaning that the central ion moves towards the surface and the outer H atoms away from it. In the LDA approximation this amounts to a difference of ∼0.4 Å. Likewise the presence of the molecule induces a small distortion in the substrate: the Ag atoms beneath the pyrole-Nitrogen ($N_p$) are shifted ∼0.1 Å below the average level, while the Ag atoms under the $N_a$ and some of the atoms under the benzene rings lie ∼0.1 Å above the average. The molecule-substrate distances $z$, shown in Table 4.1, have been calculated as the difference in the $z$ coordinate between the TM atom and the Ag atom below the $N_p$. The distance obtained with LDA is ∼2.5 Å for all the four molecules. This functional is known to over-bind, only indirectly compensating for vdW forces, which are not included in the calculations.

The GGA+vdW functional provides a way to directly consider vdW forces, and by comparing plain GGA and GGA+vdW, we can further characterize the effect of the interaction between the TM ion and the substrate. In plain GGA (see Table 4.1), both FePc and CoPc are significantly closer (~0.5-0.8 Å) to the surface than NiPc and CuPc. The stronger TM-Ag interaction of FePc/CoPc is attributed to a direct participation of metal $d$ orbitals in the interaction with the substrate [150, 151]. Once the vdW interaction is introduced all distances equalize independently of the TM. The vdW correction to the total energy can be quantified: for NiPc and CuPc it is roughly 1 eV bigger than for FePc. The vdW thus compensates the lack of direct interaction via the TM ion and explains the TM-independent results of a binding distance of ~2.7 Å (Table 4.1). Similar values were found for CoPc adsorbed on Cu(111) using these methods [152]. On less reactive Au(111) surfaces, however, the distances obtained with LDA for different MePcs do not level out and still reflect a TM-dependent behavior [150].

### 4.2.2. Orbital specific electronic chirality

STM images taken at different bias voltages reveal an opposite chirality for the two molecular orientations (+30°, -30°) of NiPc/CuPc (see Figure 4.3). According to the clockwise and counterclockwise rotation of the ligand

| | LDA | GGA | GGA+vdW | $z(C_A - C_B)$ |
|---|---|---|---|---|
| FePc | 2.43 | 2.76 | 2.66 | 0.06 |
| CoPc | 2.51 | 3.08 | 2.71 | 0.05 |
| NiPc | 2.53 | 3.59 | 2.73 | 0.03 |
| CuPc | 2.46 | 3.47 | 2.66 | 0.05 |

**Table 4.1.:** Computed height distances $z$ (in Å) between the TM ion and a Ag atom in the substrate, obtained within different DFT approximations, and height difference between $C_A$ and $C_B$ atoms at the end of the benzene ring (see Figure 4.2b) obtained with LDA.

axis with respect to the [011] surface vector, these enantionmers will be denoted as r (right) and l (left). The chiral contrast depends on the bias used for imaging. At negative voltages it is clearly visible and progressively disappears for positive values, as shown in Figure 4.4. Such chiral contrast is only observed for CuPc and NiPc, not for CoPc and FePc. This behavior suggests that chirality in this system is mainly of electronic origin, i.e., not related to the molecule conformation.

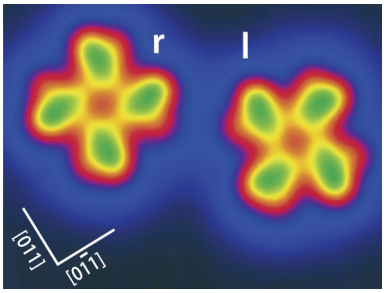


**Figure 4.3.:** STM image of CuPc adsorbed on Ag(100). Molecules rotated by $\pm 30°$ with respect to the [011] crystallographic direction show r and l chirality. (0.1 nA, -0.3 V, 5.8 nm x4.4 nm)

Both the molecule and the substrate posses a four fold symmetry. The origin of the chirality lies in the misalignment of surface and molecular symmetry axes (see Figure 4.2). As has been observed in other systems [153, 154, 155], this induces asymmetric molecule metal interactions that can lead to chiral distortions of the molecule. However structural distortions cannot not explain the observed voltage dependency of the chiral contrast.

DFT calculations reveal more about the mechanisms behind this electronic chiral contrast. We quantify the contribution of conformational

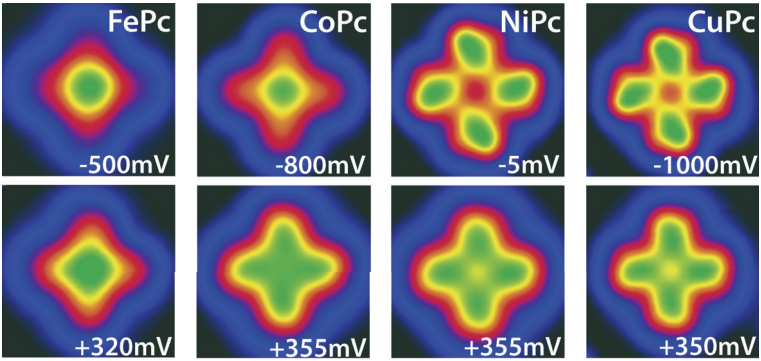


**Figure 4.4.:** Voltage dependent topographic images of all MePcs. For CuPc and NiPc negative voltage images with maximum chiral contrast are displayed. The appearance of CoPc and FePc does not vary in the range of negative voltages investigated, thus representative images are displayed. For positive voltage, all MePcs appear achiral for the studied voltage range <1 V (0.1nA, 3 nm x3 nm)

distortions in the chiral contrast. We use the height difference between two opposite C atoms at one of the benzene ring as a measure of their torsion (see Table 4.1 and Figure 4.2b). We find very small values for all MePcs, even for CoPc and FePc, which do not show any chirality in the STM images. This confirms that the chirality contrast has an electronic origin rather than a conformational one.

The DFT results show a charge transfer of roughly 1 electron into the molecule, as well as a strong hybridization between molecular and substrate states. The symmetry of electronic structure will therefore be based on the both substrate and molecule. This structural arrangement of molecule+surface is itself chiral due to the rotation of the molecule (Figure 4.2 b), hence leading to "chirally" perturbed molecular frontier orbitals, without any structural distortion.

This electronic chirality is imprinted to each molecular orbital (MO) to a different degree, depending on their spatial distribution and interaction with the substrate. The effect is mainly observed in orbitals exhibiting a nodal plane in the ligand axis (see Figure 4.5 ). The $a_{1u}$ (~ gas phase HOMO) exhibits the strongest distortion, promoted by its double lobe structure at the benzene ring. The chiral contrast at the $2e_g$ (~ gas phase LUMO), also with nodal planes at the ligand axis, varies with energy and is strongly

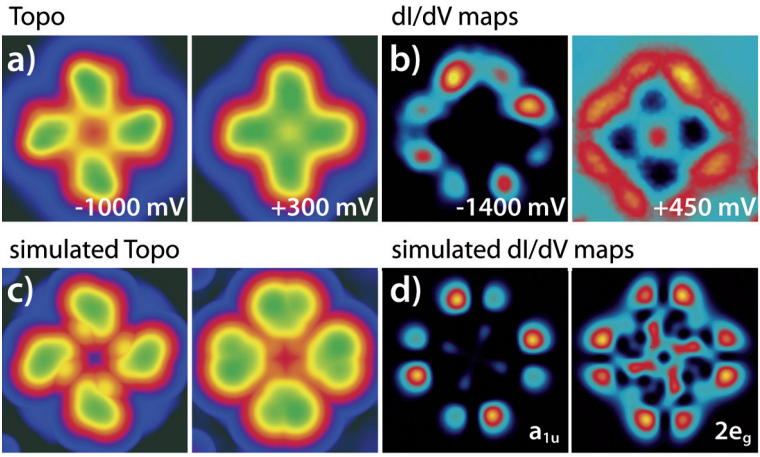


**Figure 4.5.:** Origin of the chiral contrast for: a) Voltage dependent topographic images of CuPc b) Constant current $dI/dV$ maps taken at the positions of $a_{1u}$ (~ gas phase HOMO) and $2e_g$ (~ gas phase LUMO) c) calculated STM images using DFT corresponding to the topographies in a). d) Theoretical conductance maps at the peak position of the $a_{1u}$ and $2e_g$.

reduced at positive bias. TM $d$ states and orbitals without such nodal planes do not exhibit any significant chirality. This orbital specificity leads to a bias voltage dependent chiral appearance of the MePcs depending only on the particular electronic structure of the molecule in question (see Figure 4.4). The CuPc and NiPc appear strongly chiral at negative bias, due to the presence of asymmetric orbitals, namely the $a_{1u}$ and a partially occupied $2e_g$ (see chapter 5, page 79). In contrast at positive bias the tunneling occurs through the more symmetric $2e_g$ resonance, hence no chirality is observed. On the other hand the TM $d$ orbitals and other interface related resonances with maximum intensity at the ligand hinder the observation of the chirality of the $a_{1u}$ for CoPc and FePc (see Figure 4.4). Note that the $dI/dV$ maps of the CoPc's $a_{1u}$ orbital do indeed confirm its chirality, as can be seen in the map taken at -1.5 V in Figure 5.3 on page 87.

## 4.3. Monolayer growth

We have seen that single MePc molecules adsorbed on Ag(100), have a chiral electronic structure. A key question is whether the chirality of the individual molecules can be transferred to supramolecular organizational structures. For that to occur each enantiomer must form domains consisting only of one handedness. Chiral molecules have intrinsically some kind of stereospecific interaction (hydrogen bonds[156, 157], or lateral vdW forces), facilitating the formation of supramolecular chiral domains. In the case of achiral molecules the selectivity required can be provided by the interaction with the substrate, which makes it possible to form chiral clusters. This is done by asymmetric molecular interactions due to a mismatch between molecule and substrate symmetry axis, and or lattice constraints [155, 154].

We studied the evolution of supramolecular structures for the CuPc/Ag(100) system by investigating higher coverages from dimer up to the complete monolayer. These results are contrasted to CoPc layers to determine possible effects of the central metal ion.

### 4.3.1. Evolution of chirality in CuPc and CoPc structures

STM topography images with increasing coverage of CuPc illustrate the evolution of the organizational chirality during the self-assembly process (see Figure 4.6). The mechanisms behind each step are schematically illustrated in Figure 4.7.

As a first observation, we notice that CuPc dimers mainly form with molecules of the same handedness, while mixed configurations with r and l molecules are rare. This is the signature of a chiral recognition process occurring on the single molecule level.

To answer the question whether this chirality is transferred to the supramolecular level, we consider the smallest homochiral structure. The dimer has four possible bonding configurations, which express its two levels of chirality: the individual determined by the orientation of the molecules (r or l) and the organizational, meaning the position of the molecules relative to each other. The ligand axis of one molecule can either be placed on the right or on the left of the other. These structural orientations will be denoted with capital letters R and L, depending on the rotation of the superlattice with respect to the molecular axis (see Figure 4.8 on page 68). Consequently the four structures are rR, rL, lL,

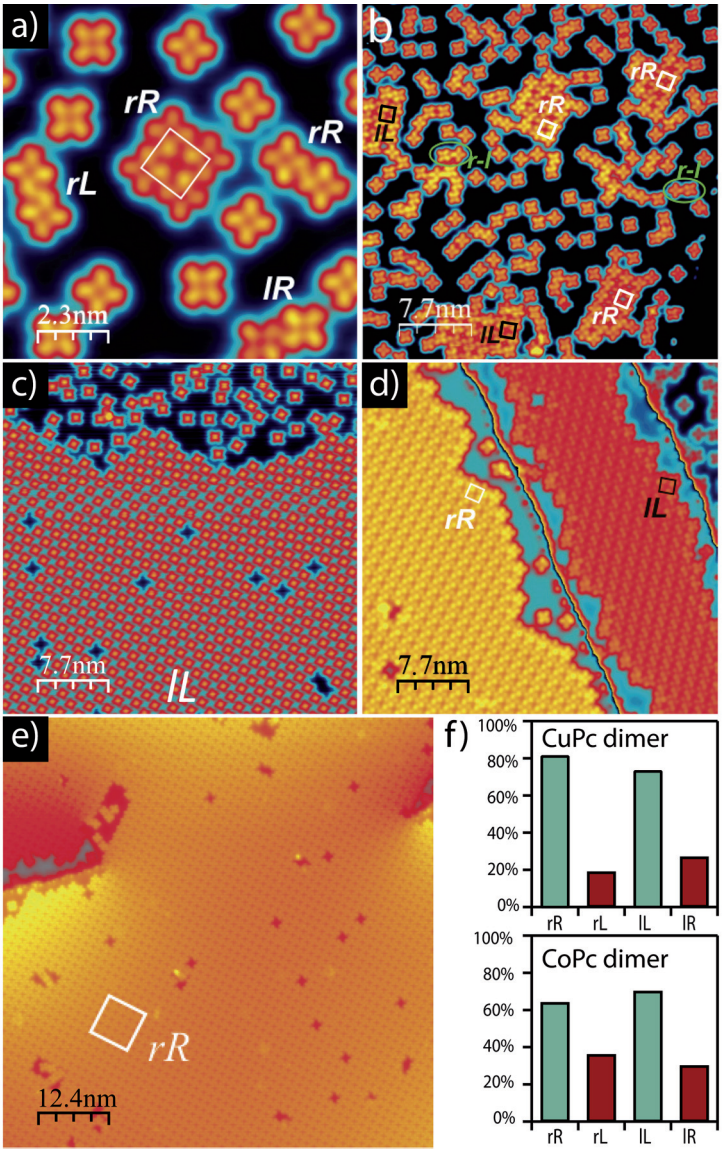


**Figure 4.6.:** Coverage dependent evolution of organizational chirality: a) At very low coverages, small clusters nucleate due to attractive intermolecular interactions. Dimers are found in all possible bonding configurations. b) At intermediate coverage, chiral recognition occurs for larger clusters, leading to a racemic mixture of either rR or lL structures. c) Ostwald ripening favors the growth of one type of domain, leading to spontaneous symmetry breaking. d) At monolayer completion, chiral purity is achieved on each terrace. e) Homochiral rR domain extending over a terrace and crossing a screw dislocation. 77.3 nm x77.3 nm f) Probability to find a dimer of each configuration for CuPc (~100 counted dimers) and CoPc (~100 counted dimers). All images are CuPc/Ag(100) except for c) which is CoPc/Ag(100), the setpoint was (0.1 nA, -1 V).

lR (see Figure 4.7 and Figure 4.6a). When we quantify the probability to encounter a certain type of dimer, it becomes clear that they are not evenly distributed: type rR and type lL dimers occur far more often than lR or rL (see Figure 4.6f). Hence a transfer of chirality from the single to supramolecular level is already present for two molecule clusters favoring rR and lL arrangements. The energy difference between these configurations, which is due to the interaction with a single neighbor, is not yet large enough to completely suppress the formation of the metastable rL/lR structures. Once the number of nearest neighbors (NN) is larger than 1 the suppression is complete. For tetramers structures with 2 NN and larger clusters with 4 NN, only rR and lL organizations are observed (Figure 4.6b). This statistic distribution of these clusters is a racemic mixture, consistent with the fact that these structures are energetically equivalent.
The behavior of CoPc is very similar, despite the non-chiral topography appearance. All clusters with NN >1 are found in the rR or lL configurations. In Dimer structures, however, the general trend of preferring rR and lL, is less pronounced (see Figure 4.6f). This might either be an empirical problem, as the total number of counted dimers was less than in the CuPc case, or due to the weaker vdW interaction (see Table 4.1) and/or $2e_g$ hybridization (see section 5.2 on page 83) with the substrate in CoPc compared to CuPc. This could allow slight rotation of the former in order to minimize the energy cost of the less favorable configurations (lR or rL). vdW interactions do not only affect the molecule-substrate separation, but also the self assembly, leading to similar organizational structures for the different MePc .

At coverages above approximately 0.5 ML, large islands of either rR or lL type develop on each terrace (Figure 4.6), growing at the expenses of the smaller ones. Near the completion of the monolayer, each terrace consists of only one enantiopure domain phase (Figure 4.6d). This Ostwald ripening process occurs due to the continuous exchange between the molecular clusters and a two-dimensional “gas” of adsorbed molecules, similarly to what is known to occur for metal systems [158]. It amplifies small initial fluctuations in the population of rR and lL enantiomers.

For this homochiral growth mechanism it is essential that the molecules can switch chirality during diffusion by rotating over the surface. This is made possible by the achiral nature of the molecules, and their high mobility on surface, when deposited at room temperature. The low energy

barrier for a molecule to switch chirality, i.e., rotate, is also reflected in tip induced diffusion experiments, where the molecule repeatedly changes the azimuthal adsorption angle during the lateral diffusion.

Mechanisms that enhance random imbalances in chirality during crystallization are essential to understanding chiral selection processes that take place in nature. In general complete spontaneous symmetry breaking is a rare process for molecules to occur in solution [159, 160]. On surfaces the constrained growth in two dimensions can be used to induce spontaneous chiral growth. However, usually only a racemic mixture of domains is obtained [161, 131, 162]. Enantiopure molecular layers require an external driving force, such as enantiomeric excess [159], a chiral modifier [160], chiral solvent [163], or magnetic field [164]. Here we presented a case where symmetry breaking of chiral molecular layers occurs spontaneously, and is complete at the single terrace level. The extension of the homochiral layers is thus limited only by the morphology of the substrate, not by kinetic or thermodynamic effects.

### 4.3.2. Supramolecular structure

We have determined the supramolecular structure of the self assembled CuPc monolayer/cluster by STM. Figure 4.8 show two high resolution STM images of the to observed chiral domains.

Let us consider these structures in more detail for the case of the l enantiomer. The same arguments hold true for the r type. The superlattice structure that we observe for the l molecule, shown in Figure 4.8 c), is lL, which is commensurate with the surface with a 5x5 periodicity. We find that in the superlattices the angle between molecular and surface symmetry axes reduces slightly from $\beta$ = -30° to -27° as compared to the single molecules (negative sign corresponds to counterclockwise, i.e., left, rotation). A similar reduction of the azimuthal angle is also observed in the relaxed structures obtained in the calculations.

The lL superlattice consists of a square unit cell, rotated by $\alpha = -26.1°$ with respect to the molecular axis direction, meaning $\alpha + \beta$= -27°-26.1° =$\gamma$= -53.1° rotation with respect to the surface primitive vectors. Due to the 4-fold symmetry of the surface this is equivalent to a -53.1°+90° = +36.9° rotation, which defines the rotation angle in the reference frame of the surface. In Wood's notation, the lL superstructure would then be written as 5x5R37°, whereas in matrix notation, using the basis of the surface unit cell, the same structure is expressed as

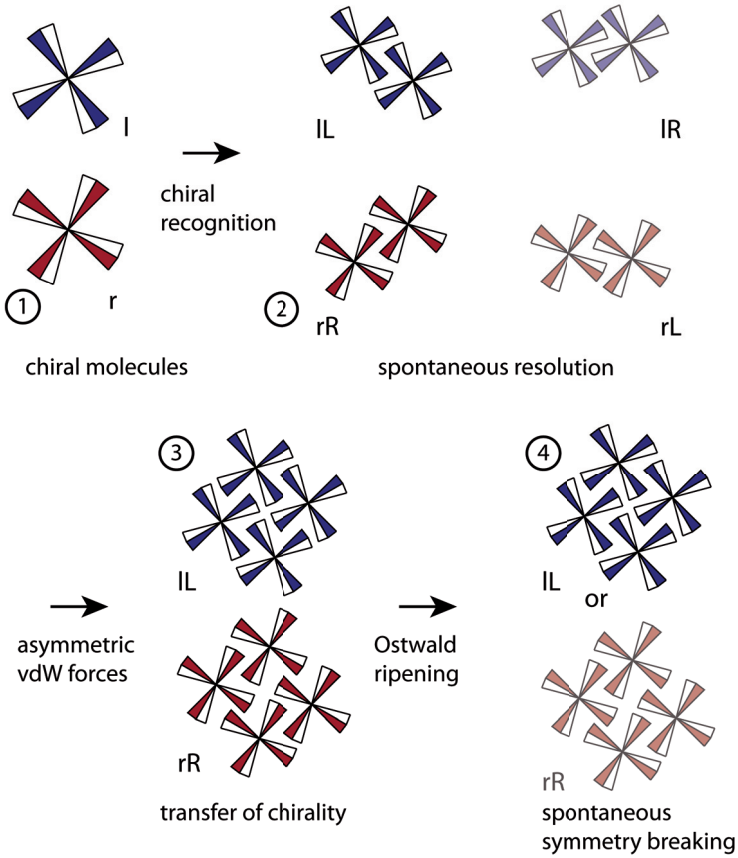


**Figure 4.7.:** Schematics of the self-assembly mechanisms that induce homochirality on the CuPc/Ag(100) surface. The combination of adsorbate-substrate matching and vdW interactions is strong enough to induce chiral recognition (phase separation of r and l molecules), and transfer the chirality from the single-molecule level to the organizational level (r/l forming only rR/lL islands). Ostwald ripening combined with reversible single-molecule chirality favors the homochiral growth of the largest cluster at the expense of the smaller ones, leading to spontaneous 100 % enantiomeric excess on each terrace.

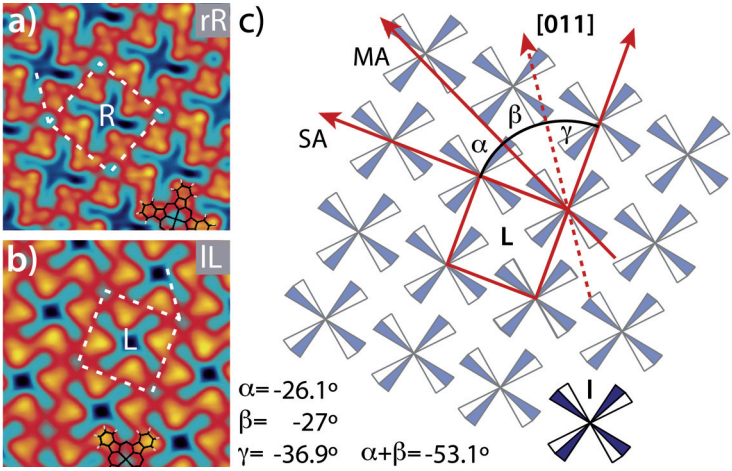


**Figure 4.8.:** Detailed STM topographies of the chiral clusters (a) rR and (b) lL domains recorded with $V_b$ = +0.52 V and -0.10 V respectively (0.1 nA). (c) The lL superlattice configuration. The molecular axis (MA) and superlattice unit cell directions (SA) and angles with respect to the [011] surface direction are superposed.

$$M_{lL} = \begin{pmatrix} 4 & 3 \\ -3 & 4 \end{pmatrix} \tag{4.1}$$

Maintaining the nomenclature for the dimer, we use the letter L to denote its chirality in reference to the counterclockwise (left) rotation of the superlattice unit cell with respect to the molecular axis.

The corresponding mirror symmetric superstructure (lR) would be rotated by +26.1° with respect to the molecular axis, leading to a unit cell closely aligned (-27° + 26.1° = -0.9°) with respect to the primitive vectors of the Ag(100) surface. The equivalent superlattice matrix is:

$$M_{lR} = \begin{pmatrix} 5.001 & 0.087 \\ -0.087 & 5.001 \end{pmatrix} \tag{4.2}$$

Evidently, this structure is not commensurate with the surface. Because the molecule-substrate interaction dominates over intermolecular forces,

the molecules accommodate to the surface lattice, forming a slightly modified 5x5 superstructure. The closest commensurate superlattice corresponds to a rotation of the unit cell by +27° with respect to the molecular axis, hence a 5x5R0° structure or:

$$M_{lR} = \begin{pmatrix} 5 & 0 \\ 0 & 5 \end{pmatrix} \tag{4.3}$$

We have thus found the four possible superlattice structures: for the l enantiomer lL 5x5R37° repectively lR 5x5R0° and for the r orientation 5x5R-37° for rR and 5x5R0° for rL. Note that the latter structure coincides with lR, however the molecules are a different enantiomer, i.e., rotated in the opposite direction.

In the low temperature STM images only the most stable configurations lL and rR were observed, as the system was slowly cooled. By fast freezing small rL/lR clusters were occasionally created (Data not shown). In low energy electron diffraction (LEED) experiments at room temperature, all of these four domains are found to be coexisting. The broad spot at 0° in Figure 4.9 indicate the presence of rL/lR clusters with short range order. The fact that all of them are presences suggest a small energy difference between rL/lR and lL/rR cluster, which confirmed in the next section by DFT.

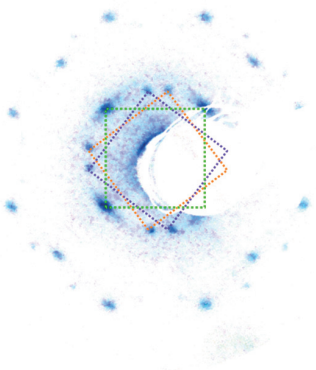

**Figure 4.9.:** LEED pattern for CuPc/Ag(100) recorded at room temperature showing the coexistence of rR (orange), lL (blue), and rL/lR domains (green square).

### 4.3.3. Origin of the transfer of chirality

The energetics and mechanisms involved in the formation of chiral supermolecular clusters can be understood through DFT calculations for the lL and lR structures. Two possible pathways, which have been found to cause chirality in molecular clusters on surfaces were considered: Substrate mediated interactions and direct vdW interaction between molecules.

#### 4.3.3.1. Substrate-mediated molecular interactions

Substrate mediated interactions can lead to chiral recognition due to long-range Coulomb forces combined with adsorption site constraints [165, 166]. Previous theoretical investigations have shown this to occur for molecules with proper gas-phase chiral conformation, i.e., tartaric acid adsorbed on Ni(100) [167] and phenylglicine on Cu(110) [165, 166]. To investigate the role of these forces for MePc on Ag(100), our collaborators P. Ordejón and N. Lorente have modeled the adsorption of single CuPc molecules in a huge 15x15 supercell to avoid possible periodic boundary effects (SIESTA). Indeed the electron density of the Ag atoms surrounding the molecule show a chiral perturbation of the metal states resulting in a distortion of the electrostatic potential around the molecule ( Figure 4.10).

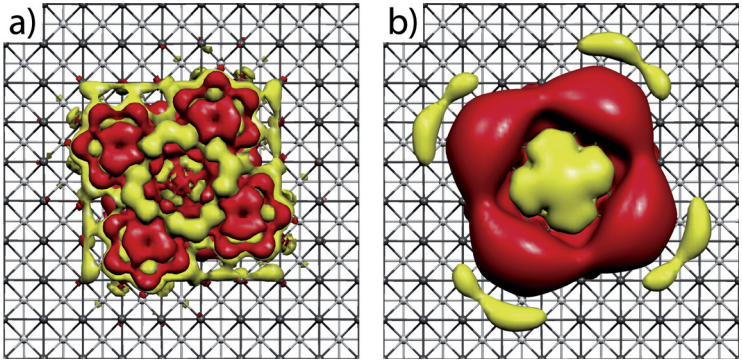


**Figure 4.10.:** (a) Extended differential electron density and (b) electrostatic potential of an l oriented CuPc molecule adsorbed on a 15x15 supercell (only partially shown). The contours correspond to values of ±7x10-4 $e/\AA^3$ and ±0.07 eV for the density and potential, respectively. Yellow (red) indicates positive (negative) values

The potential is asymmetric up to a distance of about 15 Å from the Cu

ion, which is larger than the distance to the benzene ring of the nearest neighboring molecule (13 Å), suggesting a possible influence in the chiral recognition process. We integrated the induced electrostatic potential at the position that would be occupied by a second molecule in the lL and lR adsorption sites. The electrostatic interaction energy of one molecule due to the presence of the other one is given by:

$$E_{el} = \int \rho_{tot}(\vec{r}) \cdot V_H(\vec{r}) d\vec{r} \tag{4.4}$$

where, $\rho_{tot}$ represents the total charge density of the second molecule (sum of electronic and nuclear charges), $V_H$ is the electrostatic potential induced by the first molecule, and $\vec{r}$ the position. Note that, for such large molecules, a fully self-consistent calculation where the two molecules are included in the computation of the potential is at present prohibited by the supercell size limitations. After integration over the region occupied by the second molecule we find a negligible energy difference of $\Delta E = E(lL) - E(lR) = 3.5$meV. Our $\Delta E$ is about one order of magnitude smaller than the substrate-induced interaction estimated for opposite phenylglicine enantiomers and adenine on Cu(110) [165, 166]. Moreover these molecules have a much smaller surface footprint compared to MePc, suggesting that the effect of substrate-mediated interactions between enantiomers depends not only on charge transfer but also on the size of the adsorbates. In conclusion due to the small energy difference, we can exclude substrate-mediated molecular interactions as the driving force behind the chiral recognition process.

#### 4.3.3.2. Intermolecular van-der-Waals forces

The second pathway we considered were intermolecular van-der-Waals forces. To compute the contributions to the chiral recognition, two different functionals were used, following the same arguments used for the adsorption of single molecules (see page 59). LDA reproduces the TM-substrate interactions quite well, however weak interactions like vdW are only indirectly described. The second functional DSRLL is designed specifically to work with vdW forces and hence should provide a more accurate description. Using both functionals, the relaxed structures and energies for the two configurations (lL and lR) were obtained.

The structure of the monolayer is mainly determined by the interaction between each individual molecule and the Ag(100) surface. The angle

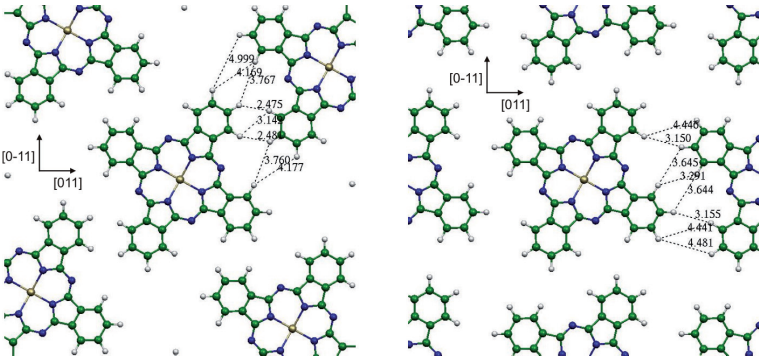


**Figure 4.11.:** Scheme of the structure of the lL (left) and lR (right) monolayers (Ag atoms are not shown for the sake of clarity), indicating the contact distances between neighbour molecules. Results obtained with the DSRLL functional.

between the molecular symmetry axes and the substrate crystallographic directions in the relaxed structures is essentially the same for both structures (see Figure 4.11), indicating that intermolecular interactions in the monolayer are less important than molecule-surface interactions. This is the case for both of the DFT functionals used.

However, the contact distances between neighboring molecules are different for the lL and lR structures. This is due to the fact that both assemblies have the same angle between molecule and substrate axes and the same 5x5 superlattice periodicity, whereas the unit cell vectors are different. As a consequence, neighboring molecules lie in different directions. The intermolecular contacts are shorter for the monolayer in the lL phase, as shown in Figure 4.11, because the relative orientation between molecules is such that two phenyl groups are closer in this case.

| | LDA | DSRLL | DSRLL no vdW |
|---|---|---|---|
| $\Delta E$(ML on Ag100) | -69 | -41 | 3 |
| $\Delta E$(free ML) | -94 | -74 | 16 |

**Table 4.2.:** Energy differences between the lL and the lR structures $\Delta E = E(lL) - E(lR)$ in meV, computed with different DFT functionals. Negative values indicate a preference for the lL phase.

Finally in Table 4.2 the energy differences between the lL and lR phases are shown. If the vdW contributions are not considered (DSRLL no vdW) both structures are energetically almost equal. This means that (i) the energy of interaction between the molecule and the surface is similar in both structures, due to the similarity in the angles discussed previously; (ii) the molecules are sufficiently far so that the repulsive part of the interactions (which is present in the calculation) is negligible, and (iii) the effect of the interaction between molecules through the electronic states of the metal does not play an important role in the energy difference between the phases.

However, once vdW forces are included, the two chiral structures become separated by 41meV, which clearly identifies vdW interactions as the driving force for the chiral interaction. These (attractive) vdW forces between neighboring molecules are stronger in the lL phase due to the slightly closer distances between the molecular endgroups.

It is interesting to note that the energy difference between both phases is smaller for the monolayer over the metallic surface than for the free monolayer, by almost a factor of two. This may be due to a screening of the vdW interactions by the metallic surface [168], hereby reducing the effect on the total energies as well as the energy difference. The LDA results show the same tendencies as those obtained by DSRLL, albeit with larger energy differences. This is a known shortcoming; LDA tends to overestimate the binding at short distances in vdW complexes.

## 4.4. Multilayer growth

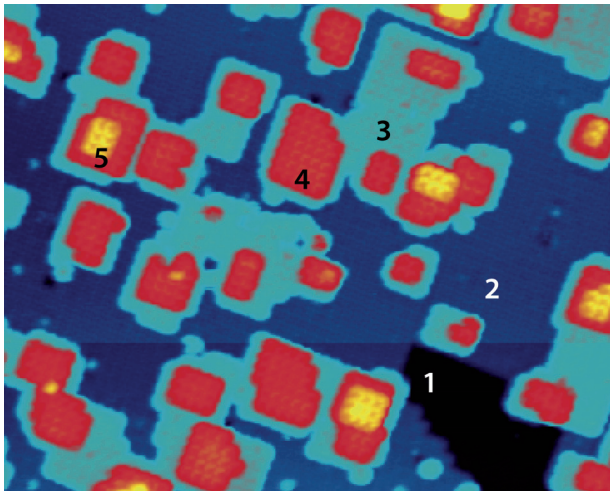


**Figure 4.12.:** Overview image indicating the different molecular layers marked 1-5.(77 nm x49 nm, 10 pA, 1.5 V )

We investigated the growth behavior of CuPc beyond the first monolayer. In order to do this the sample preparation differs slightly. The first monolayer was deposited at room temperature. It acts as a wetting layer and completely covers the surface of the sample in the manner described in subsection 4.3.1. We then deposited the following layers at 77 K in order to grow stacks of up to 5 molecular layers in a Stranski-Krastanov growth mode, as seen in Figure 4.12. A similar growth mode has been observed for SnPc on Au(111) [145] and FePc on Ag(111) [129].

The adsorption configuration is different in each layer (see Figure 4.13). The molecules of the second layer lie flat on the first layer molecules, with the central Cu ions still aligned, and the ligand axis azimuthally rotated by 45°, as has been seen for CoPc multilayers [140].

On the third layer, flat lying molecules coexist with ones slightly tilted out of the surface plane. By comparing the molecular sizes in topographic images, this tilt can be estimated: $\beta$=5° for the 3$^{rd}$ layer (see Figure 4.13d). Additionally and independently of the tilt, part of the molecules experience a shift of the position of the central TM ion, $\alpha \approx 43° \pm 10°$. On the 4$^{th}$ and 5$^{th}$ layer all molecules are titled by $\beta$=7° and respectively $\beta$=8°, as

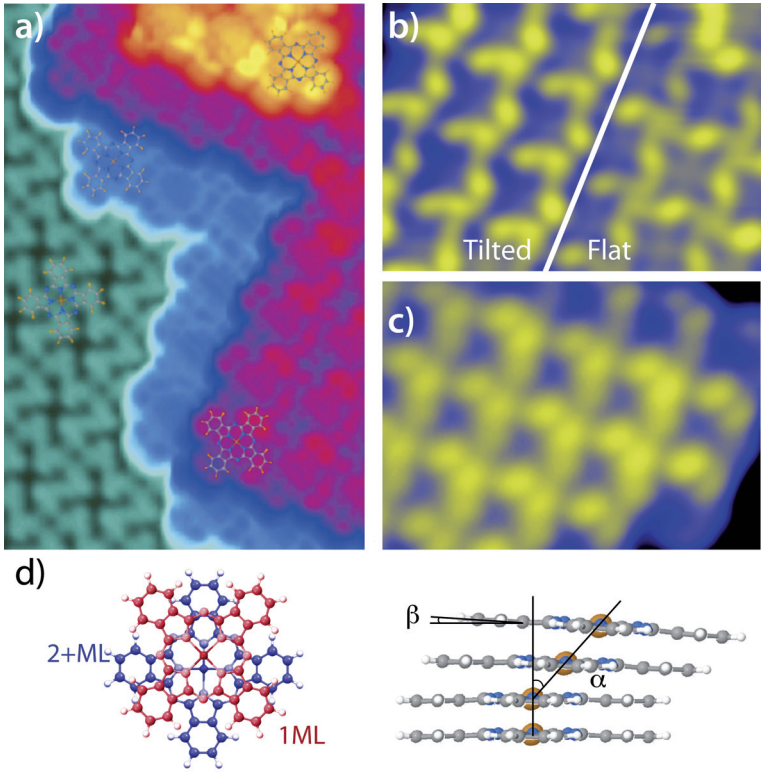


**Figure 4.13.:** Topographic STM images of the Multilayer adsorption of CuPc on Ag(100) a) Pseudo-colored zoom. Molecules indicate the adsorption geometry (14 nm x9 nm, 20 pA,1.5 V) b) Zoom of molecules in the 3$^{rd}$ layer, showing the tilted and flat adsorption c) Zoom of molecules in the 4$^{th}$ layer, here all molecules are tilted d) Schematics of the multilayer adsorption: starting form the 2$^{nd}$ layer the ligand axis is rotated by 45°, in higher layers the molecules are tilted and off-centered.

well as shifted.

The tilted/shifted adsorption geometry is driven by $\pi$-$\pi$ interaction of neighboring molecules, which becomes increasingly stronger due to

weaker influence of the substrate-molecule interaction. Ultimately the configuration found in bulk MePc crystals is reached. This behavior has been observed in several other multilayer MePc systems, however depending on the strength of molecule substrate interactions it occurs already in the second layer for FePc/Ag(111) [129], CoPc/Au(111) [144] and on the first layer on NaCl [145]. The observed values agree with literature values of $\beta$=3° for the second layer and $\beta$=4° for the third layer [144]. The $\alpha$ angle lies also roughly within the range of previously observed values of $\alpha \approx$30° [140].

## 4.5. Summary

We studied the adsorption with varying coverage of four MePcs (Me = Fe, Co, Ni, Cu) on Ag(100) using scanning tunneling microscopy and comparing them to ab-initio calculations.

**Single molecule adsorption**: All four single MePc molecules independent of the TM show the same configuration on Ag(100). The $\pi$ interaction between the macrocycle and the substrate leads to a flat adsorption geometry with the center metal ion situated on a Ag hollow site. The bond optimization between the aza-Nitrogen and the Ag substrate atoms results in two possible orientations of the molecular axis rotated by $\pm$30° with respect to the [011] surface vector.

**Single molecule chirality**: The molecular adsorption configuration is chiral, due to the mismatch between molecular and surface symmetry axis. This imprints chirality to the frontier molecular orbitals without perturbing the structural conformation of the molecule. The degree of distortion of the MO depends on their symmetry and spatial distribution. The $a_{1u}$ orbital and the $2e_g$ are the most affected, the former more so. This orbital specific chirality can be disentangled in $dI/dV$ maps. This can be observed as chiral contrast in topography images for NiPc/CuPc at negative bias, because the only contribution to the tunneling current comes from chiral orbitals ($a_{1u}$). For FePc/CoPc the existence of a filled achiral MO hinders this contrast .

**Monolayer growth**: We studied higher coverages of CuPc and CoPc, to investigate the self assembly. The molecules grow in clusters, with a 5x5 periodicity. Further we find that the molecules express chirality on

a supramolecular level. At low temperatures we observe two different chiral domains.

**Transfer of chirality**: We find that within these clusters asymmetric vdW interactions lead to the transfer of chirality from single molecule level to the organizational. The origin of the asymmetry lies in the mismatch between molecule and substrate symmetry axis in combination with a lattice matching constraint imposed by molecule-substrate interactions. Because these interactions are vdW, the transfer of chirality does not dependent on the TM ion. This mechanism should hold true for all four MePc. The strength of these vdW forces depends on the number of neighboring molecules. In CuPc and CoPc dimer structures the transfer of chirality is not yet perfect, however once a second neighbor is added it becomes univocal.

**Homochirality**: For the complete monolayer of CuPc we observe homochiral growth. This spontaneous symmetry breaking is based on the Ostwald ripening of smaller clusters, made possible by the thermally induced molecular rotations that switch the chirality of single MePcs during the deposition at room temperature. Since vdW ligand interactions are the driving force, this result should be general for all four MePc.

**Multilayer adsorption**: By first depositing a wetting layer of MePc at RT, and subsequent deposition of additional layers at 77K, we have studied the evolution of self assembly of up to 5 multilayer of CuPc on Ag(100). The molecules grow in in a Stranski-Krastanov growth mode. On the $2^{nd}$ layer the molecular axis is rotated by 45° while maintaining the alignment of the TM ions between the $1^{st}$ and $2^{nd}$ layer. A gradual tilting from the surface plane occurs. On the $3^{rd}$ layer molecules that are slightly tilted coexist with ones in flat configurations, while on higher layer all molecules are tilt. The gradual tilting reflects how, in absence of the stronger molecule-substrate interaction, the molecules prefer to organize in the closed packed structure observed in bulk films, with vertical stacks bonded by $\pi$-$\pi$ interactions.